Petroleum Science 18 (2021) 1492–1506

Contents lists available at ScienceDirect

Petroleum Science

journal homepage: www.keaipublishing.com/en/journals/petroleum-science

Original Paper

Preparation and properties of magnesium oxysulfate cement and its application as lost circulation materials

Kai-Xiao Cui [a], Guan-Cheng Jiang [a, *], Li-Li Yang [a], Zheng-Qiang Deng [a, b], Lei Zhou [c]

[a] State Key Laboratory of Petroleum Resources and Prospecting, MOE Key Laboratory of Petroleum Engineering, China University of Petroleum (Beijing), Beijing, 102249, China
[b] CCDC Drilling Fluid Technical Service Company, Chengdu, 610056, Sichuan, China
[c] Zhundong Drilling Company of CNPC Xibu Drilling Engineering Company Limited, Karamay, 834000, Xinjiang, China

ARTICLE INFO

Article history:
Received 29 August 2020
Accepted 26 April 2021
Available online 20 August 2021

Edited by Yan-Hua Sun

Keywords:
Magnesium oxysulfate cement
Lost circulation material
Severe loss
Acid soluble plug
Formation damage

ABSTRACT

Loss of drilling fluids in large porous and fractured zones inevitably up-regulates the overall cost of drilling. As a type of acid-soluble cement, magnesium oxysulfate (MOS) cement is arousing huge attention for the less hygroscopic nature and less damaging to steel casings compared with magnesium oxychloride (MOC) cement. The present study developed MOS cement as a fast setting, high strength and acid-soluble lost circulation material to reduce the problem of losses. As suggested in this study, a higher strength of MOS cement at 70 °C could be achieved by elevating $MgO/MgSO_4 \cdot 7H_2O$ molar ratio or down-regulating $H_2O/MgSO_4 \cdot 7H_2O$ molar ratio. Boric acid and borax could act as effective retarders. Plugging slurry based on MOS cement could effectively block the simulated porous loss zones exhibiting a diameter from 1.24 mm to 1.55 mm, as well as the fractured loss zones with a width from 2 mm to 5 mm and bearing a pressure difference up to 8 MPa. Permeability recovery test demonstrated that it facilitated future oil and gas production. The successful field application in the Junggar Basin, Xinjiang, China verified the significant plugging effect of MOS cement for severe loss problems.

1. Introduction

Drilling operation is recognized as the first vital process to access oil and gas resources and geothermal reservoirs. During drilling, circulating drilling fluids exhibit several fundamental functions, which include applying of stress on the borehole wall to prevent borehole instability (breakouts or collapse), removal of cuttings generated by the drill bit from the borehole, acquiring information from the drilled formation, elevating rate of penetration, as well as cooling and lubricating of the drill bit (Johannes, 2012; Li et al. 2015, 2018; Caenn et al., 2017; Werner et al., 2017). Loss of circulation may occur in the presence of large intergranular pores, natural or induced fractures, or caves in the formation drilled (Elkatatny et al., 2020). Lost circulation may cause a heavy financial cost and extend the non-productive time, thereby generating serious environment hazards and leading to the abandonment of the wells; in the worst case, it can even cause safety accidents (Howard and Scott, 1951; Onyia, 1994; Alkinani et al. 2020). There are four types of losses given their severity (the loss rate), which are elucidated as (I) seepage losses (loss rate below 1.6 m^3/h), (II) partial losses (1.6–16 m^3/h), (III) severe losses (above 16 m^3/h), and (IV) total loss (no return to surface) (Lavrov, 2016). On the whole, seepage and partial losses could be reduced by directly adding conventional lost circulation materials (LCMs) (e.g., nutshell (NS) (Chellappah et al., 2018), sized calcium carbonate and resilient graphitic carbon (RGC) (Kumar et al. 2010), rubbers (Nayberg, 1987), cellulosic fiber (CF) (Alsaba et al., 2014b)) into the drilling fluid at different concentrations while drilling. However, under severe or total losses, drilling should be stopped immediately, and a prepared plugging slurry should be squeezed, which includes gunk (Sugama er al. 1986), cement or deformable, viscous and cohesive plugs (DVC) (Wang et al. 2005) and others, into the loss zones, thereby forming a plug to enhance the pressure-bearing capacity of the formation, as well as ensuring no occurrence of repeated losses during the continual drilling (Xu et al., 2020). The mentioned LCMs and treatments critically alleviate the burden attributed to lost circulation events.

* Corresponding author.
E-mail address: m15600263100_1@163.com (G.-C. Jiang).

https://doi.org/10.1016/j.petsci.2021.08.002

However, defects of the mentioned LCMs are also exposed in practical field applications. Particulate LCMs (e.g., nutshells and fibers) cannot form cross-linked and stable blockings, which can be removed prematurely under severe conditions (e.g., pressure fluctuation attributed to pipe tripping and frequent washing of drilling fluids), both causing repeated losses (Nasiri et al., 2018). Moreover, high concentration and large size LCM blends may block the downhole tools (e.g., bit nozzles) (Sweatman and Scoggins, 1990). It is noteworthy that the precondition of a compact bridging layer is that the size between the LCMs and loss channels complies with a certain bridging rule (e.g., 1/3 bridging rule (Abrams, 1977), ideal packing theory (Dick et al., 2000), or Vickers method (Vickers et al., 2006)). However, the exact size characteristics of loss zones (e.g., loss type, pore diameter, or fracture width) are commonly difficult to determine immediately, so an appropriate particle size distribution (PSD) of LCMs is hard to design for an effective plugging (Whitfill and Hemphill, 2003; Savari et al. 2015). Organic cross-linked LCMs (e.g., polymers) can form a deformable, viscoelastic gel adapting and filling the loss channels; however, it develops high gel strength but no compressive or tensile strength, so it may flow away when drilling operations resume, thereby causing loss to occur (Mata and Veiga, 2004; Cole-Hamilton and Curtis, 2008). Inorganic cross-linked LCM (e.g., cement) is the mostly used treatment for partial to total losses, with a high cost (over $60,000) and relatively high probability of success (over 70%), as indicated from lost circulation treatment data of over 2000 wells drilled worldwide (Alkinani et al., 2020). On the whole, the high cost of cement plug results from the large usage amount and long waiting on cement time. More importantly, the cement plug may irrevocably damage producing zones for its low acid solubility (Cole-Hamilton and Curtis 2008). As revealed from the mentioned defects, better LCMs should be developed to further improve the plugging performance and down-regulate the treatment cost.

To overcome the mentioned defects, acid soluble cements (ASCs) as a loss treatment solution were developed. Over the past decades, a wide range of ASCs have been studied, (e.g., magnesium oxychloride (MOC) cement and conventional cement containing acid soluble components). MOC cement (i.e., a mixture of magnesium oxides and magnesium chlorides) exhibits the advantages of quick setting, early strength, high strength, as well as brine corrosion resistance. Vinson et al. reported MOC cement to be an acid removable cement system to reduce severe losses in producing zones (Vinson et al. 1992). Subsequently, Bour et al. modified the mentioned cement to a low density ASC system by foaming (Bour et al., 1993). Moreover, Ravi employed MOC cement as an acid soluble plugs in open-hole slotted-liner completion (Ravi 2010). Based on the specific laboratory investigation, Seymour and Santra compared the properties of MOC cement and Portland cement based system with $CaCO_3$ in an appropriate amount (Seymour and Santra 2013). The weakness of MOC cement comprises poor water resistance, high moisture absorption, high deformability, as well as a tendency to corrode steels (Wu et al., 2014; Zeng et al., 2019). Consistent with MOC cement, magnesium oxysulfate (MOS) cement also shows the merits of rapid setting, early strength, and high acid solubility, which is in contrast to Portland cement (Li and Ji, 2015; Walling and Provis, 2016). It arouses huge attention for the less hygroscopic nature of magnesium sulfate as opposed to magnesium chloride (Jeroch, 1906; Rueff, 1907; Stewart, 1932), thereby enabling easier shipping and a longer shelf life for bagged cements (Walling and Provis, 2016). Commonly, MOS cement has a lower strength impacted by the limited solubility of $MgSO_4 \cdot 7H_2O$ at ambient temperature, which can be effectively improved by elevating temperatures or by introducing modifying additives (Qin et al., 2018; Zeng et al., 2019). The development of MOS cement based on sulfates indeed avoids the use of chlorides, making them less damaging to steel (Walling and Provis, 2016). Furthermore, MOS cement can more effectively comply with the requirements of energy conservation and environmental protection, the topics fully advocated in the development of modern society and human technology progress. This is explained as magnesium oxide, one of the main raw materials of MOS cement, only requires magnesite to be calcined at nearly 900 °C. In contrast, the clinker of Portland cement should be calcined at higher temperature of 1450 °C (Zeng et al., 2019).

MOS cement is basically composed of MgO, $MgSO_4$ solution and appropriate retarders. The compressive strength is primarily determined by the type, relative content and microstructure of hydration products ($xMg(OH)_2 \cdot yMgSO_4 \cdot zH_2O$ phases), as significantly impacted by the molar ratio of MgO, $MgSO_4$ and H_2O, as well as temperature. Demediuk and Cole comprehensively studied the MgO–$MgSO_4$–H_2O system at the temperature from 30 to 120 °C and then concluded the phase equilibria (Fig. 1) (Demediuk and Cole, 1957). To be specific, they identified four magnesium oxysulfate phases, i.e., $3Mg(OH)_2 \cdot MgSO_4 \cdot 8H_2O$ (3-1-8 phase), $5Mg(OH)_2 \cdot MgSO_4 \cdot 3H_2O$ or $2H_2O$ (5-1-3 phase or 5-1-2 phase), $Mg(OH)_2 \cdot MgSO_4 \cdot 5H_2O$ (1-1-5 phase) and $Mg(OH)_2 \cdot 2MgSO_4 \cdot 3H_2O$ (1-2-3 phase). Elevated temperature increases the solubility of $MgSO_4$, prompting the precipitation of the 1-1-5 and 1-2-3 phases which contain higher proportions of $MgSO_4$. Later researchers focus on studying the phase composition of MOS cement at ambient temperature for better applications in construction industry. Newman concluded that the 3-1-8 phase was the only stable phase generated at 25 °C (Newman, 1964). Urwongse and Sorrell also found that the 3-1-8 phase was the main phase formed at 23 °C along with $Mg(OH)_2$ and hydrated forms of $MgSO_4$. The mentioned conclusions were in agreement with the results reported by Demediuk and Cole that only 3-1-8 phase and $Mg(OH)_2$ exist at 30 °C (Urwongse and Sorrell, 1980). However, for applications in the oil and gas industry, the phase composition at higher temperatures from 40 to 120 °C is important for analyzing the variation of compressive strength after solidification in the downhole conditions.

In the present study, the effect of raw materials molar ratio on compressive strength development, phase composition and microstructure of MOS cement were discussed in detail. Then, the retarding effect of three kinds of retarders (citric acid, boric acid and borax) for MOS cement was compared. Its acid solubility to hydrochloric acid (HCl) was measured under different acid

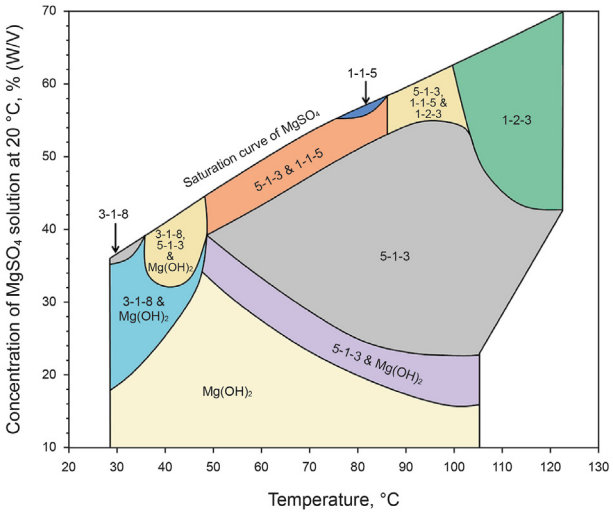

Fig. 1. Phase equilibria in the MgO–$MgSO_4$–H_2O system (Walling and Provis, 2016).

concentrations and durations. To fully exploit its advantage of early strength, MOS cement was added directly to the drilling fluids to transform it into a fast settable plugging slurry. Its plugging performance for simulated large cavernous zone and fractured zone was evaluated. Furthermore, a core permeability recovery test was performed to evaluated the degree of formation damage. The research shows that MOS cement can provide a convenient, fast and efficient way to solve losses.

2. Materials and methods

2.1. Raw materials

Light-burned magnesia powder (MgO, industrial reagent, purity ≥87%) was purchased from Hebei Magnesium Chemical Technology Co. Ltd. (China). The main impurities included $MgCO_3$ and SiO_2. It had a mean particle size of 12.095 μm, and a hydration activity of 53.7% (see **Appendix** for details). The BET surface area is 15.85 m^2/g. Magnesium sulfate heptahydrate ($MgSO_4 \cdot 7H_2O$, purity ≥99%) was a colorless fine needle-like crystal offered by Zhengzhou Jiahong Chemical Products Co., Ltd. (China). Anhydrous citric acid ($C_6H_8O_7$, analytical reagent, purity ≥99%), boric acid (H_3BO_3, analytical reagent, purity ≥99%) and borax ($Na_2B_4O_7 \cdot 10H_2O$, analytical reagent, purity ≥99%) acted as the retarders. All the mentioned retarders were purchased from Energy Chemical (China). The drilling fluid additives comprised bentonite (BT), sodium hydroxide (NaOH), poly(acrylamide-acrylic acid) potassium salt (K-PAM), sulfonated asphalt (SA), poly(2-acrylamido-2-methylpropane sulfonic acid, sodium salt-N, N-dimethylacrylamide-acrylonitrile) (RSTF) (David and Charles, 1986), low viscosity polyanionic cellulose (PAC-LV), calcium carbonate ($CaCO_3$ with a mean particle diameter of 44 μm), potassium chloride (KCl) as well as barite ($BaSO_4$). All the mentioned additives were offered by Beijing Shida Bocheng Technology Co., Ltd. (China).

2.2. MOS cement slurry preparation

The MOS cement slurry was comprised of $MgSO_4 \cdot 7H_2O$, MgO and H_2O. The $MgSO_4 \cdot 7H_2O$ was dissolved in deionized water to form a solution. Subsequently, the necessary amount of MgO powder was slowly added to the solution and then blended for a few minutes to prepare MOS cement slurries. A range of varied MOS cement slurries exhibiting different molar ratios of MgO:$MgSO_4 \cdot 7H_2O$:H_2O were prepared.

2.3. Compressive strength measurement and phase composition analysis

Fig. 2a presents 2 cm × 2 cm × 2 cm cubic samples for each MOS cement slurry formulation prepared by curing in a custom steel mold with vibration compaction. Subsequently, the mold was placed in a water bath at 70 °C for 24 h. The compressive strength was recorded by measuring average crush strength of three cubes for the respective sample with WDW-100Y uniaxial compression apparatus (Jingzhou Modern Petroleum Science and Technology Co., Ltd. (China)) (Fig. 2b) under a maximum force of 10 kN at 50 N/s loading rate. Similar evaluation methods have been adopted by other researchers (Seymour and Santra 2013; Li et al., 2017). Specific to crystal-phase composition analysis, the MOS cement was ground to a powder to acquire X-ray diffraction (XRD) patterns, collected on an X-ray diffractometer (PANALYTICAL (Netherlands)) through the identification of Powder Diffraction File card number (PDF card no.) (Gates-Rector and Blanton, 2019), with CuKα radiation and 30 kV of acceleration voltage condition over a 2θ range of 5°–90°. Furthermore, the microstructures were characterized under a SU8010 scanning electron microscope (SEM) (HITACHI (Japan)) on fractured surfaces after gold coating.

2.4. Setting time measurement

The setting time of MOS cement slurries was determined by performing the penetration test with the SZR-5 penetration tester (Hebei Kebiao Instrument Co., Ltd. (China)) (Wang et al., 2019). The penetration of the MOS cement slurry was defined as the depth of the standard needle (50 g load) falling freely in 5 s into the MOS cement slurry at 70 °C. A deeper penetration indicates a softer specimen and a smaller consistency. Boric acid, borax, and anhydrous citric acid were used as retarders, and their retarding performance was determined.

2.5. Acid solubility test

Acid solubility experiments can be impacted by a range of parameters (e.g., setting time, specimen size, acid type, acid concentration and treatment time) (Luke and Soucy, 2008). The acid in this test was limited to HCl since it is the most commonly used one in acid treatment. The MOS cement was soaked in the HCl solution to determine the effect of HCl concentration and immersion time on the acid solubility. The specimen of MOS cement with MgO:$MgSO_4 \cdot 7H_2O$:H_2O of 10:1:30 and 20% boric acid as retarder was ground into 6–10 mesh size. Subsequently, 2.0 g of dried specimen was placed in a test tube at 70 °C, and 14 mL of the HCl solution (mass concentration of 10%, 15%, 20%, and 25%) was poured into the respective test tube. After a certain period, the remaining MOS cement particles were filtered and then dried to a constant weight; next, the acid solubility (%) was calculated by the following equation (Luke and Soucy, 2008; Jadhav and Patil 2018):

$$S = \frac{m_1 - m_2}{m_1} \times 100\% \quad (1)$$

where S denotes the acid solubility, %; m_1 and m_2 are the initial weight of the MOS cement particles and the weight of remaining MOS cement specimen after being dried, respectively, g.

2.6. Plugging evaluation experiment

The in-situ field drilling fluid obtained from an oil field in the Junggar Basin, Xinjiang, China was taken as the basic fluid. Table 1 lists the specific formula of the drilling fluid with a density of 1.4 g/cm^3 weighting with barite.

Two methods were used to prepare MOS plugging slurries: one was prepare by dissolve $CaCO_3$ (filling agent) in distilled water; the other was prepared with the drilling fluid obtain from an oil field. The design principles of the MOS plugging slurries prepared from in-situ drilling fluid were as follows. (1) MgO and $MgSO_4 \cdot 7H_2O$ as chemical solidification additives were added to the drilling fluid at different proportions to improve the compressive strength. (2) The setting time of the MOS plugging slurry was optimized by retarders to satisfy to the operation requirement. The effect of MOS cement on viscosity and gel strength of the drilling fluid was evaluated with a direct-indicating viscometer (Qingdao Tongchun Oil Instrument Co., Ltd. (China)) referring to API Recommended Practice 13B-1 (American Petroleum Institute, 2009).

The plugging performance of plugging slurries was evaluated with a high temperature high pressure (HTHP) fluid loss apparatus (Qingdao Tongchun Oil Instrument Co., Ltd. (China)) (Alsaba et al., 2014a). To be specific, two-layer steel ball beds formed by steel balls of different diameters (D) were used to simulate the porous loss zones. According to the three-sphere packing model, the

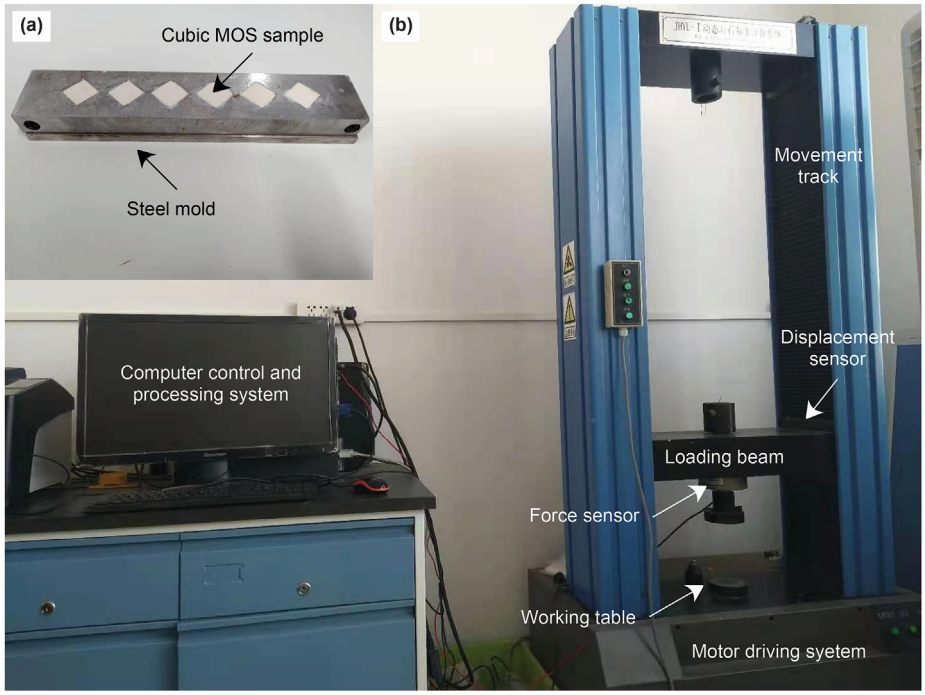

Fig. 2. Compressive strength measurement of MOS cement. **(a)** Custom steel mold for the preparation of MOS cubic cement samples. **(b)** Uniaxial compression apparatus.

Table 1
The specific formula of the drilling fluid from an oil field in the Junggar Basin.

Additives	Function	Concentration, kg/m^3
BT	Viscosity increaser	30
NaOH	pH-modifier	2
K-PAM	Viscosity increaser and borehole stabilizer	2
SA	Sealing agent	30
RSTF	Filtrate reducer	20
PAC-LV	Viscosity increaser	5
$CaCO_3$	Sealing agent	20
KCl	Inhibitor	50

diameter of the inner pore is 0.1547 times the diameter of the ball (Wang, 2007). Straight slotted discs of different widths were used to simulate the natural fractured loss zones. Table 2 lists the typical simulation methods for different loss channel types in laboratory. The physical model of the plugging evaluation is shown in Fig. 3.

2.7. Permeability recovery test

The HTHP fluid loss apparatus was also used to determine the efficiency of removal of MOS cement by 15% HCl solution (Mata and Veiga 2004). To simulated the porous producing formation, a corundum disc with dimensions of 5.36 cm × 0.6 cm (diameter × thickness) was used. The 2% hydroxyethyl cellulose (HEC) solution with a viscosity of 81.5 mPa·s was used as the test medium. The experimental procedure is described as follows. (1) In a baseline test established, the original permeability of the corundum disc was measured by injecting 2% HEC. By recording the outlet flow rate under a certain pressure difference, the original permeability of the corundum disc was calculated according to the Darcy's law (Ahmed, 2010). (2) The corundum disc was then plugged by injecting 12 mL MOS cement (10:1:30). After it cured, the plugging permeability of the corundum disc to 2% HEC was tested. (3) The corundum disc was taken out and soaked in 200 mL 15% HCl solution for 2 h at 70 °C to dissolve the MOS plugging layer. (4) The corundum disc was reloaded and the restored permeability was tested. The permeability calculation formula was as follows:

$$k = -\mu \frac{Q}{A} \frac{\mathrm{d}L}{\mathrm{d}p} \tag{2}$$

where k denotes the permeability of the porous corundum disc, D; μ represents the viscosity of the flowing fluid, mPa·s; Q is the flow rate through the porous corundum disc, cm^3/s; A is the cross-sectional area of the corundum disc, cm^2; dL is the axial length of the corundum disc, cm; dp is the pressure difference between the inlet and outlet of the drilling cup, 10^{-1} MPa.

Table 2
Typical simulation methods for different loss channel types in laboratory.

Loss channel types	Simulation Methods	Steel ball diameters or slotted disc widths	Pore diameters or fracture widths
Large pores	Two layer steel ball beds	8 mm	1.24 mm
		9 mm	1.39 mm
		10 mm	1.55 mm
Large fractures	Straight slotted disc with a smooth wall	2 mm	2 mm × 6 mm
		3 mm	3 mm × 6 mm
		4 mm	4 mm × 6 mm
		5 mm	5 mm × 6 mm

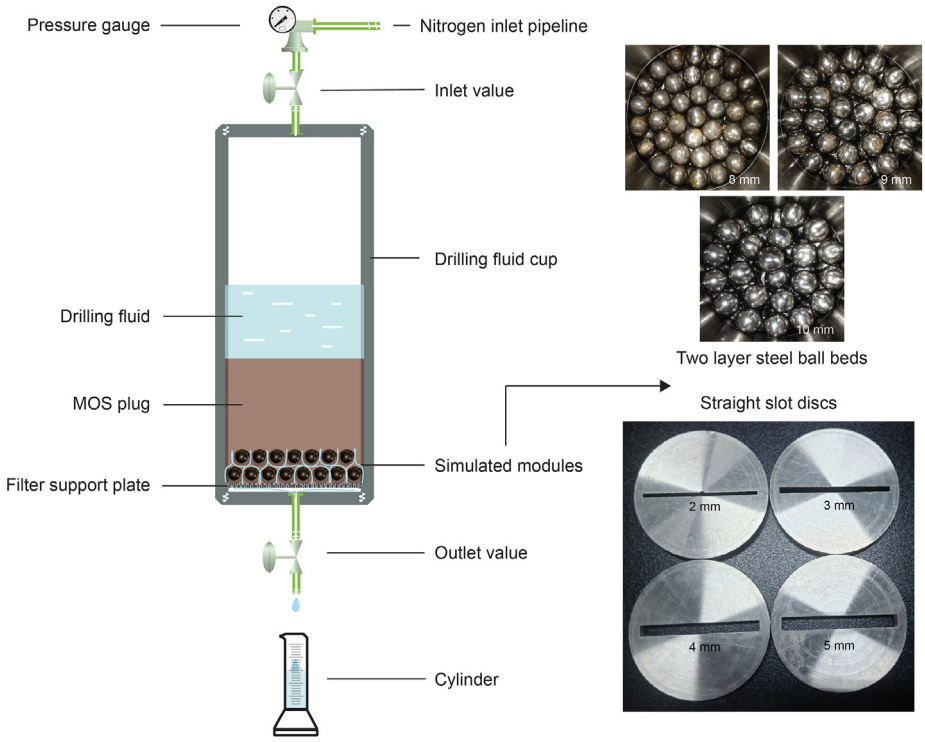

Fig. 3. The physical model of plugging evaluation.

3. Results and discussion

3.1. The compressive strength development mechanism of MOS cement

When MOS cement acts as the lost circulation material, high compressive strength of MOS plug can help improve the bearing capacity of the loss zone. The compressive strength of MOS cement depends on the crystal-phase composition and microstructure, which is largely impacted by the proportions of the raw materials (Beaudoin and Ramachandran, 1978; Li and Ji, 2015).

3.1.1. Effect of raw materials molar ratio on the compressive strength of MOS cement

To determine the effect of the $MgO/MgSO_4{\cdot}7H_2O$ and $H_2O/MgSO_4{\cdot}7H_2O$ molar ratio on the compressive strength, several MOS cement slurries of different $MgO/MgSO_4{\cdot}7H_2O/H_2O$ molar ratios (i.e., 5:1:12, 6:1:12, 7:1:12, 8:1:12, 9:1:12, 10:1:12, 10:1:21, 10:1:30, 10:1:50, 10:1:70, and 10:1:90) were prepared. Fig. 4 illustrates the change in the compressive strength of MOS cement as function of $MgO/MgSO_4{\cdot}7H_2O$ molar ratio from 5:1 to 10:1 and $H_2O/MgSO_4{\cdot}7H_2O$ molar ratio from 15:1 to 90:1. It is shown that the compressive strength of MOS cement rises with the increase in the $MgO/MgSO_4{\cdot}7H_2O$ molar ratio and decreases with the increase in the $H_2O/MgSO_4{\cdot}7H_2O$ molar ratio. So, the effect of molar ratio on compressive strength of MOS cement at 70 °C is in good agreement with the results at ambient temperature (Li and Ji, 2015; Qin et al., 2018). This indicates that a higher compressive strength could be obtained by increasing MgO content or reducing H_2O content in MOS cement.

3.1.2. Phase composition and microstructure

The difference between the strength among the mentioned MOS cements may due to the different phase assemblages of the reaction products. A healthier crystals growth, better formation, compact structures and higher efficiency of the constituent consumption could result in higher physical strength. The XRD patterns of the mentioned MOS cements are illustrated in Fig. 5a and Fig. 6a. It shows that the crystal phases of the mentioned MOS cements after curing at 70 °C for 24 h are primarily composed of $5Mg(OH)_2{\cdot}MgSO_4{\cdot}2H_2O$ (5-1-2 phase) (PDF card no. 86–1322), $Mg(OH)_2$ (PDF card no. 82–2453) and MgO (PDF card no. 77–2364). MOS cement with $MgO/MgSO_4{\cdot}7H_2O/H_2O$ molar ratio of 8:1:12 exhibits stronger peak intensity of 5-1-2 phase and weaker peak intensity of $Mg(OH)_2$ and MgO. The 5-1-2 flake phases (Fu et al.,

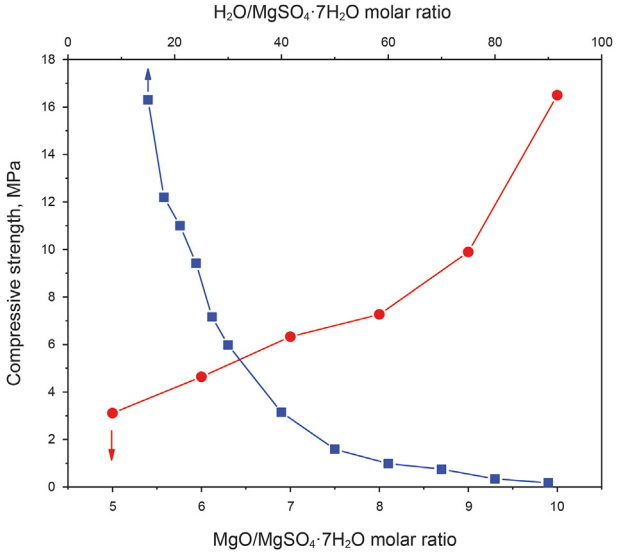

Fig. 4. Compressive strength of MOS cement of different $MgO/MgSO_4{\cdot}7H_2O$ and $H_2O/MgSO_4{\cdot}7H_2O$ molar ratios after curing at 70 °C for 24 h.

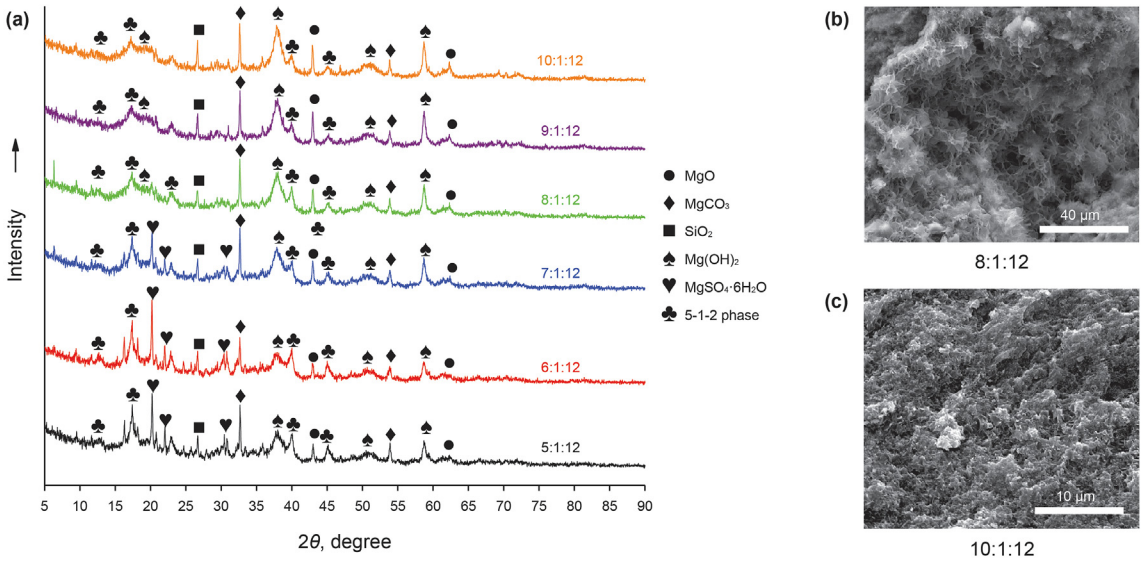

Fig. 5. XRD patterns and SEM images of MOS cement exhibiting different molar ratios of $MgO/MgSO_4{\cdot}7H_2O/H_2O$: **(a)** XRD patterns (5:1:12, 6:1:12, 7:1:12, 8:1:12, 9:1:12, 10:1:12); **(b)** 8:1:12 of SEM image; (**c**) SEM image of 10:1:12.

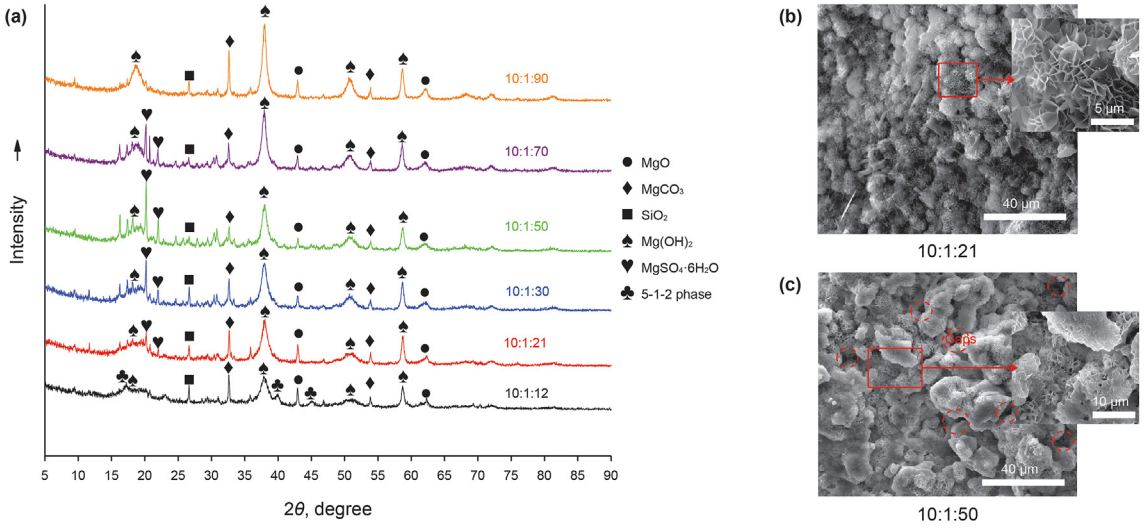

Fig. 6. XRD patterns and SEM images of MOS cement of different molar ratios of $MgO/MgSO_4{\cdot}7H_2O/H_2O$ after curing at 70 °C for 24 h: **(a)** XRD patterns (10:1:12, 10:1:21, 10:1:30, 10:1:50, 10:1:70 and 10:1:90); **(b)** SEM image of 10:1:21; **(c)** SEM image of 10:1:50.

2011) could be seen in Fig. 5b. The peak intensity of MgO and $Mg(OH)_2$ increased and no significant change was identified in the peak intensity of 5-1-2 phase while the molar ratio of $MgO/MgSO_4{\cdot}7H_2O$ increased from 5:1 to 10:1 and the molar ratio of $H_2O/MgSO_4{\cdot}7H_2O$ was fixed at 12:1. MOS cement with $MgO/MgSO4{\cdot}7H_2O/H_2O$ molar ratio of 10:1:12 exhibited stronger peak intensity of $Mg(OH)_2$ and MgO and weaker peak intensity of 5-1-2 phase, demonstrating that the MgO was not completely consumed by the reactions and generates more $Mg(OH)_2$. The residual MgO (low reactivity or excess amount) could act as the fillers and improves the compactness (Li and Ji, 2015), making the MOS cement denser and more compact (Fig. 5c), thereby enhancing the compressive strength. This resulted in the raise of compressive strength, while the $MgO/MgSO_4{\cdot}7H_2O$ molar ratio was up-regulated (Fig. 4).

As the $H_2O/MgSO_4{\cdot}7H_2O$ molar ratio increased from 12:1 to 90:1 and the $MgO/MgSO_4{\cdot}7H_2O$ molar ratio was fixed at 10:1, the peak intensity of $Mg(OH)_2$ increased significantly while the peak intensity of 5-1-2 phase and MgO decreased in the MOS cement. Though the increase in H_2O content facilitated the formation of $Mg(OH)_2$ (Wang et al., 2018), the decrease in $MgSO_4$ concentration inhibited the 5-1-2 phase from being formed, thereby causing the crystal phases from completeness (Fig. 6b) to incompleteness (Fig. 6 c). Moreover, the gaps between hydration products were extended (Fig. 6b and c), which reduced the connectivity and the compactness (Li and Ji, 2015). The absence of the 5-1-2 phase and lack of filling effect of the excess MgO resulted in a decrease of compressive strength of MOS cement, as verified in Fig. 4. As indicated from the mentioned results, lower molar ratio of $H_2O/MgSO_4{\cdot}7H_2O$ and higher molar ratio of $MgO/MgSO_4{\cdot}7H_2O$ more significantly contribute to the formation of MOS cement with better compressive strength.

Moreover, $MgSO_4{\cdot}6H_2O$ (PDF card no. 72–1068) existed in some MOS cements, probably acting as the product of $MgSO_4{\cdot}7H_2O$

losing one water molecule as impacted by insufficient dissolution. The $MgCO_3$ and SiO_2 in the MOS cement originated from the impurities of MgO. They did not exert any impact on the hydration reaction since no distinct change in peak intensity was identified among the mentioned MOS cements.

3.2. Effect of different retarders on setting time

The setting time comprises the initial and final setting time, displaying a tight relationship to the variation in rheological properties of cement slurry. It is generally required to complete the slurry preparation and the pumping and tripping process before initial solidification ensuring the safety. The drilling operations can continue after final solidification. For plugging slurries, appropriate initial and final setting time helps shorten the plugging period and lower the cost.

Fig. 7a plots the penetration depth versus time of MOS cement slurry without adding retarder. Within 16 min, it remained a liquid state with a maximum penetration depth of 40.0 mm. Since 18 min, the slurry solidified rapidly, and the penetration drastically decreased. After 26 min, the slurry was completely solidified, which developed a certain initial strength (penetration < 0.5 mm). To be specific, the time at which the slurry began to cure and finished solidification was defined as the initial setting time and final setting time, respectively. The initial and final setting time of the MOS cement slurry without retarder was only 16 min and 26 min, respectively. Fig. 7b, c and d present the setting time of MOS cement slurry at $MgO:MgSO_4{\cdot}7H_2O:H_2O$ molar ratio of 10:1:30 after the addition of different contents of retarders by weight of MgO. Specific to 20% citric acid, the initial and final setting time were 22 min and 54 min, extended by 37.5% and 107.7%, respectively. Critic acid can easily dissolve in water and form chelates with divalent and trivalent metal cations (e.g., Ca^{2+}, Mg^{2+} and Fe^{3+} ions) in the solution, probably reducing its dissolution (Ekholm et al., 2003; Müller and Tor, 2014; Ciriminna et al., 2017). However, critic acid exerted the limited retarding effect on the MOS cement at 70 °C, inconsistent with the results at low temperature (Barralet et al., 2004; Gbureck et al., 2004; Wang et al., 2019). This may be explained as its ability to chelate Mg^{2+} ions is weakened at elevated temperatures. For 20% boric acid, the initial and final setting time were 88 min and 128 min, extended by 450% and 392.3%, respectively. For 20% borax, the initial and final setting time was 52 min and 78 min, which were extended by 225.0% and 200%, respectively. The retardation is due to the Mg^{2+} chelated by $B_4O_7^{2-}$, forming a colloidal precipitate around MgO particles, reducing further dissolution (Sugama and Kukacka, 1983; Hall et al., 2001), and then retarding strength development following the known action of $Na_2B_4O_7$ as a water softener: $Mg^{2+}(aq) + B_4O_7^{2-}(aq) \rightarrow MgB_4O_7(s)$ (Arora, 2005). The retarding ability at 70 °C of the mentioned retarders was ranked as: boric acid > borax > citric acid.

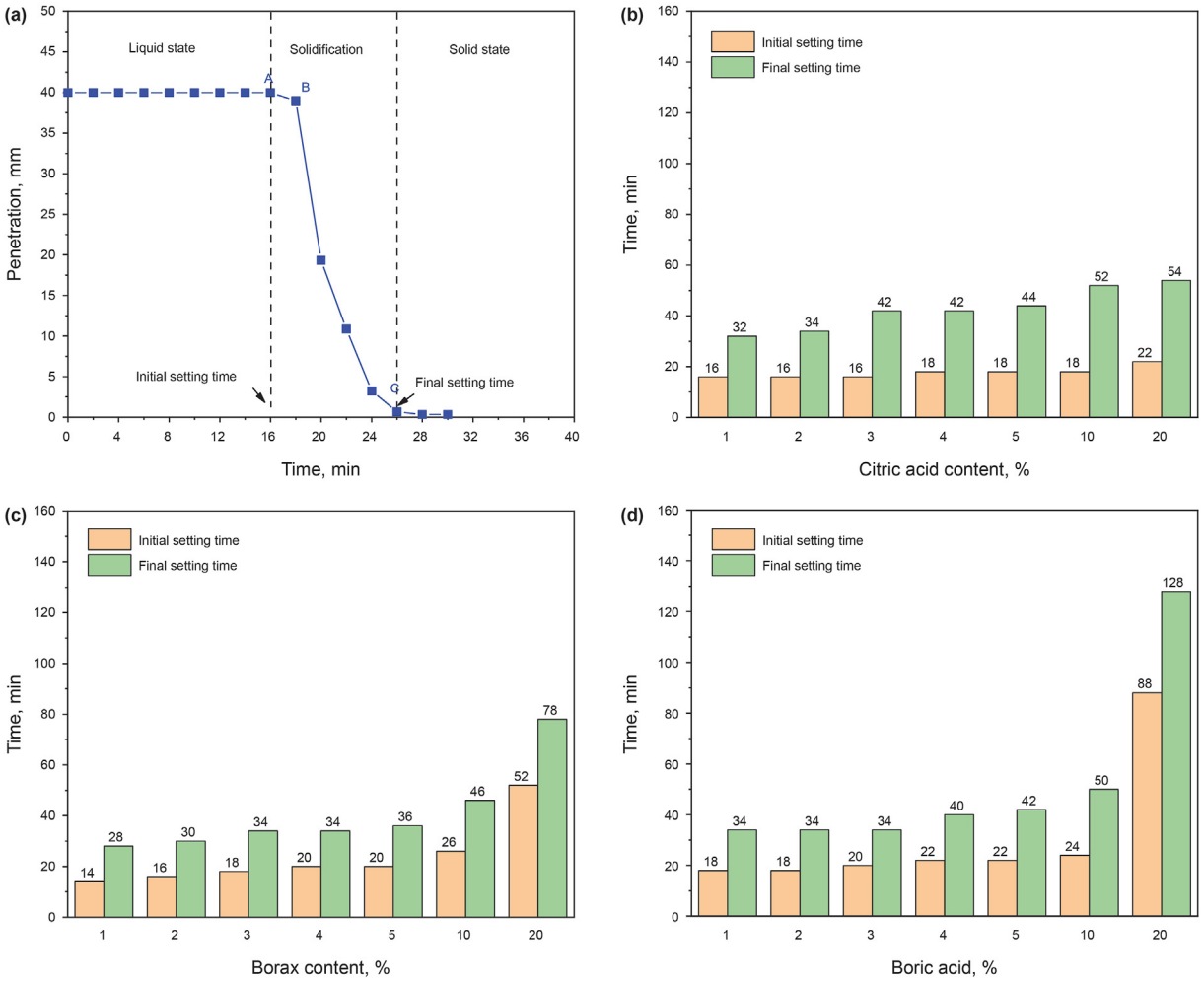

Fig. 7. Setting time of MOS cement with $MgO/MgSO_4{\cdot}7H_2O/H_2O$ molar ratios of 10:1:30 (**a**) without retarders, and added (**b**) critic acid, (**c**) borax and (**d**) boric acid.

Once the plugging slurry is prepared, pumping operation can be initiated. To be specific, three steps are involved: first, all plugging slurry is pumped into the drill pipe; subsequently, the plugging slurry is replaced out of the drill pipe into the annulus by the drilling fluid; lastly, the drill pipes are tripped out, and the slurry is waited for setting. Table 3 lists the estimation of pumping time for plugging slurry. For a loss zone located at nearly 2300 m at 70 °C, the appropriate initial setting time is estimated to be 50–90 min (longer than pumping time), and the final setting time is as short as possible. For the mentioned reason, both borax and boric acid can act as effective retarders at 70 °C.

3.3. Acid solubility

On the whole, Class G cement exhibits low acid solubility as impacted by a protective coating around the cement formed by the siliceous component that prevents further dissolution. The solubility of Class G cement can be improved by adding acid soluble components (e.g., $CaCO_3$). The solubility was 9.3% without the presence of $CaCO_3$ and 52.0% with the presence of 200% $CaCO_3$ by weight of cement in 15% HCl after 120 min (Luke and Soucy, 2008). MOS cement exhibits higher acid solubility of almost 100% compared with Class G cement. With 20% HCl and 25% HCl, MOS cement was completely dissolved into a yellow liquid phase in 5 min, and the acid solubility reached 100%. With the concentration of HCl decreasing to 15% and 10%, the acid solubility curve as a function of time was plotted in Fig. 8. With 15% HCl, the acid solubility after 150 min reached up 97.06%; when the HCl concentration declined to 10%, the acid solubility after 150 min decreased to 54.41%. The dissolution of MOS cement in HCl was attributed to reactions of the acid with $Mg(OH)_2$ and 5-1-2 phase to form $MgCl_2$ and $MgSO_4$, which are soluble in water. The reactions between MOS cement and HCl are expressed as follows:

$$Mg(OH)_2\,(s) + 2HCl\,(aq) \rightarrow MgCl_2\,(aq) + 2H_2O$$

$$5Mg(OH)_2 \cdot MgSO_4 \cdot 2H_2O\,(s) + 10HCl\,(aq) \rightarrow 5MgCl_2\,(aq) + MgSO_4\,(aq) + 12H_2O$$

The mentioned reactions essentially caused the leaching of Mg^{2+} from the cement, and the bonding phases started to decompose and disintegrate, thereby accelerating the dissolution. MOS cement would be lastly dissolved into a clear and yellow solution. The yellow color might be attributed to the presence of iron-containing impurities derived from light-burned magnesia. As also indicated from this test, extremely high HCl concentration can increase the dissolution rate and shorten the dissolution time. However, extremely low HCl concentration may cause incomplete dissolution and the remaining MOS cement may block the oil and gas flow channels, thereby reducing oil and gas production. Given the field practice, 15% HCl is expected as the most suitable acid treatment condition for the MOS cement.

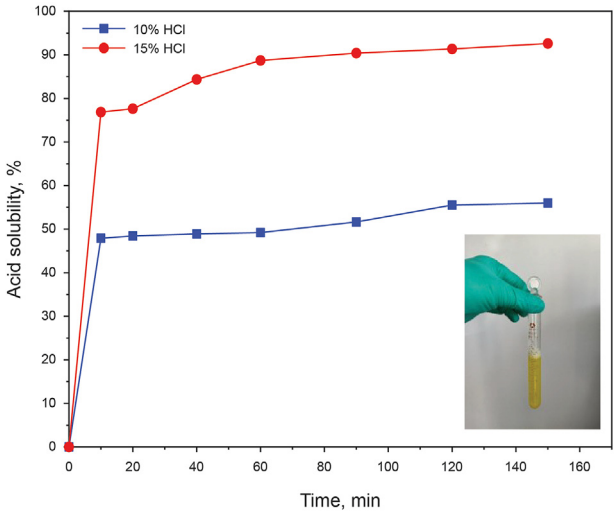

Fig. 8. Acid solubility versus time in 10% HCl and 15% HCl solutions.

3.4. Plugging performance of two types of MOS plugging slurries

3.4.1. MOS plugging slurry prepared from distilled water

According to the mentioned experimental results, the MOS plugging slurry prepared from distilled water consists of MOS cement with $MgO/MgSO_4 \cdot 7H_2O/H_2O$ molar ratio of 10:1:30 and 20% boric by weight of MgO as the retarder, with a density of 1.2 g/cm^3. The plugging ability was evaluated by performing the laboratory plugging test. Fig. 9 plots the cumulative loss volume and plugging pressure versus time of the MOS plugging slurries for blocking the porous loss zone simulated by a two-layer steel ball bed of a diameter of 8 mm at 70 °C. From Fig. 9, under the pressure lower than 1.0 MPa, the cumulative loss volume was approaching to zero; however, under the pressure higher than 1.0 MPa, the loss began to occur, and the cumulative loss volume increased with the rise of the pressure. This is explained as that the solidified MOS plug exhibits a lower permeability under a pressure difference lower than 1.0 MPa. The pressure at which the loss initially occurs, also termed as initial loss pressure, is primarily determined by the compressive strength and permeability of the MOS plug and the property of the drilling fluid. Bentonite, particulate LCMs (e.g., $CaCO_3$), and fibers can all be part of cement systems used to cure losses (Lavrov, 2016). Even if a plugging plug exhibits a high

Table 3
Estimation of pumping time for a plugging slurry

Label	Engineering parameters	Values		Notes
A	Temperature at loss zone, °C	70		/
B	Depth of loss zone, m	2333		Geothermal gradient: 3 °C/100 m
C	Pump rate of drilling fluid pump, m^3/min	2		It is related to the size of cylinder liner and pump stroke.
D	Borehole volume, m^3/100 m	3.66		8.5 inch drill bit size: 215.9 mm
E	Drill pipe inner volume, m^3/100 m	0.93		5.5 inch drill pipe inner diameter: 108.62 mm
F	Tripping out speed of drill pipes, m/min	9.75		Ignoring joints length
G	Plugging slurry volume, m^3	10.80	21.6	Two examples
H	Time for pumping plugging slurry into drill pipes, min	5.41	10.80	$H = G/C$
I	Time for plugging slurry to be replaced from the drill pipes by drilling fluids, min	10.8	10.84	$I = E(B/100)/C$
J	Tripping out height of drill pipes, m	295.08	590.16	$J = G/D \times 100$
K	Time for tripping out the drill pipes, min	30.26	60.52	$K = J/F$
L	Total plugging time, min	46.47	82.16	$L = H + I + K$

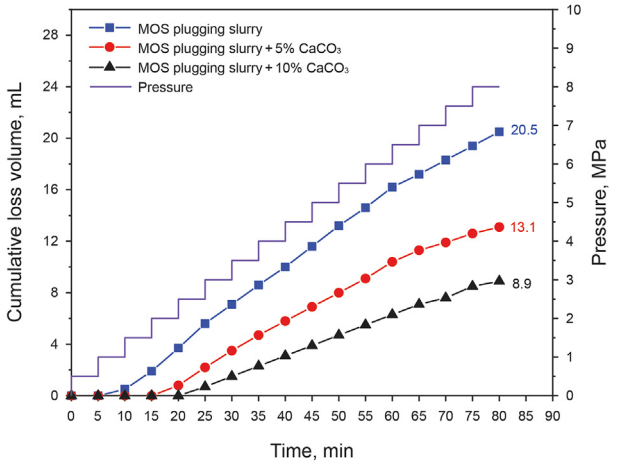

Fig. 9. Cumulative loss volume and plugging pressure versus time for blocking two-layer steel ball bed consisting of steel balls with diameter of 8 mm using MOS plugging slurry, MOS plugging slurry +5% $CaCO_3$ filling agent and MOS plugging slurry +10% $CaCO_3$ filling agent.

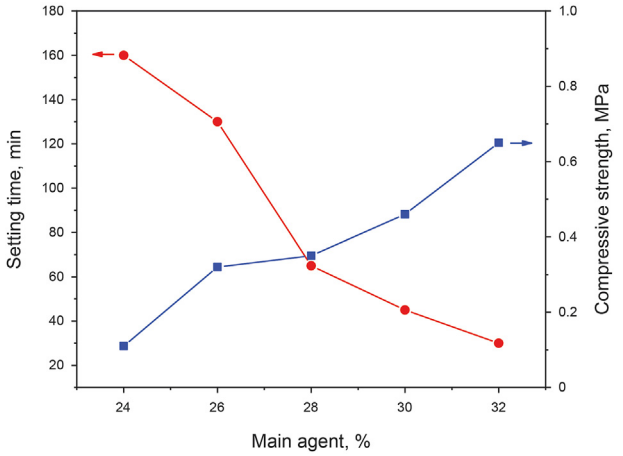

Fig. 10. Final setting time and compressive strength versus main agent ratio for the drilling fluid at 70 °C.

compressive strength, it may cause a high cumulative loss volume when its permeability is relatively large. Fig. 9 also shows that the initial loss pressure of the MOS plugging slurry increased from 1.0 MPa to 2.0 MPa with the addition of 5% $CaCO_3$ and to 2.5 MPa with the addition of 10% $CaCO_3$. Moreover, the final cumulative loss volume decreased from 20.5 mL to 13.1 mL and 8.9 mL, respectively. It is therefore indicated that the plugging effect can be further improved by increasing the compactness of the plug. The density and rheology (e.g., apparent viscosity (AV), plastic viscosity (PV), yield point (YP) and gel strength of the mentioned MOS plugging slurries are listed Table 4.

In addition to downhole temperature, the slurry density (i.e., the content of weighting agent), bentonite content (from drilling fluid pollution) and salt content (from high salinity water in loss zones) all have a significant impact on the setting time and the compressive strength of the MOS plugging system. Detailed investigations were described in reference (Cui et al., 2020).

3.4.2. MOS plugging slurry prepared from in-situ field drilling fluid

When a severe loss occurs suddenly during drilling, it is desperately expected to figure out a convenient, fast and efficient method to plug the loss zone immediately. The method that directly adding chemical solidification additives to the drilling fluid and converting it into a plugging slurry supposes to be the most promising solution. Given the mentioned idea, adding MOS cement directly to the drilling fluid to convert it into curable MOS plugging slurry refers to a fast method favored by field engineers. Here, the drilling fluid applied in oilfield was selected. The amount of main agent (MgO and $MgSO_4 \cdot 7H_2O$) and retarder were determined according to the above setting time and compressive strength measurement. In addition, economic cost should also be considered. Subsequently, the plugging ability of the solidified drilling fluid modified by MOS cement to severe losses was evaluated through the laboratory plugging evaluation.

3.4.2.1. MOS plugging slurry preparation. To evaluate the amount on plugging performance, a series of proportions (i.e., 24%, 26%, 28%, 30% and 32%) of main agent were introduced into the drilling fluid at 70 °C. Fig. 10 plots the final setting time and the compressive strength versus main agent ratio. As indicated from this figure, the curing performance of the MOS plugging slurry is related to the amount of main agent. Under the extremely low amount of main agent, the drilling fluid could not be solidified and exhibited almost no strength. This is due to too small amount of main agent which is difficult to establish an effective setting network in the drilling fluid system. When the amount of main agent is greater than 24%, the drilling fluid can be solidified as a solid plug with a certain strength. It should be noted that as the amount of main agent increases, the compressive strength raises while the final setting time of the drilling fluid is gradually shortened.

When the main agent was added at proportion of 26%, retarder (borax) under different percentages were added into the drilling fluid to investigate retardation performance at 70 °C. Fig. 11 plots the final setting time and the compressive strength versus retarder (Borax) ratio. As revealed from the result, the retarder is capable of effectively extending the final setting time of the drilling fluid. Notably, with the increase in the amount of retarder, the compressive strength decreased. Under the retarder content of 6.5%–7.5%, the final setting time was within 4.0–5.0 h. The initial setting time was 86 min under the retarder content of 6.5%, probably satisfying the requirements of drilling contractor according to Table 3. According to the mentioned optimization experiments, the MOS plugging slurry formula was determined as: the drilling fluid +26% main agent +6.5% borax. After these solidification additives were added to the drilling fluid, its flow property was affected. Table 5 lists the changes of density and rheology of the drilling fluid after adding MOS cement. Compared with the initial drilling fluid, the apparent viscosity, plastic viscosity and yield point of the slurry acceptably increased. Furthermore, the MOS plugging slurry could still be pumped directly by drilling fluid pumps. The mentioned formula was adopted for subsequent

Table 4
Density and flow properties of MOS plugging slurry prepared from distilled water.

Slurry	Density ρ, g/cm^3	Apparent viscosity, mPa·s	Plastic viscosity, mPa·s	Yield point, Pa	10″/10′ gel strength, Pa
MOS plugging slurry	1.43	25	13	11.52	7/12
MOS plugging slurry +10% $CaCO_3$	1.44	25	10	14.40	7/14

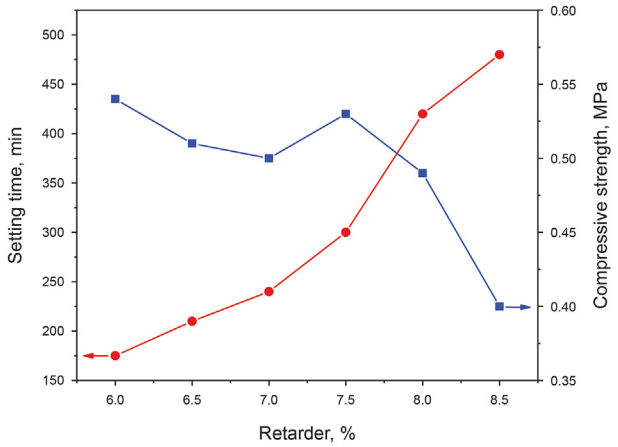

Fig. 11. Final setting time and the compressive strength versus retarder ratio for the drilling fluid containing 26% main agent at 70 °C.

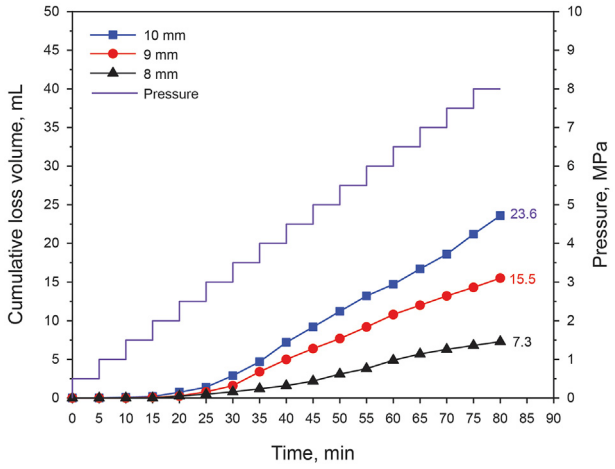

Fig. 12. Cumulative loss volume and plugging pressure versus time for blocking two-layer steel ball bed consisting of steel ball with diameter of 8, 9 and 10 mm using MOS plugging slurry.

laboratory plugging evaluation.

3.4.2.2. Plugging performance. Fig. 12 illustrates the alteration of cumulative loss volume and plugging pressure versus time using a two-layer steel ball bed (8, 9 and 10 mm) that simulates large porous loss zones. Likewise, as indicated from the figure, under the pressure lower than 1.5 MPa, the cumulative loss volume was approaching zero. Under the pressure over 1.5 MPa, the loss began to occur, and the cumulative loss volume increased with an increase in pressure. For the simulated porous loss zones of different pore sizes (1.24, 1.39 and 1.55 mm), the final cumulative loss volume of MOS plug at 8.0 MPa reached 7.3, 15.5 and 23.6 mL, respectively. In addition, the loss rate increased with the rise of the diameter of the steel balls, resulting from the larger loss channel size of the simulated loss zone. As suggested from the test result, though slight loss occurred, the MOS plug could still bear a pressure difference of 8.0 MPa between the upper and lower plug. If the loss rate was reduced to an acceptable range, the drilling could safely proceed and pass through the whole loss zone. The MOS plug (Fig. 13) forming on 10 mm steel ball bed was consistent with those solidified on the steel ball bed of other sizes. Accordingly, the MOS plugging slurry could firmly adhere to the steel balls together, which was still integrated after being taken out of the apparatus. Furthermore, the MOS plug was filled in the pores between the steel balls blocking the loss channel, so the loss was reduced.

Fig. 14 plots the cumulative loss volume curve when using the straight slotted disc with widths from 2 to 5 mm. As indicated from the figure, the initial lost pressure was nearly 0.5 MPa, and the loss rate also increased with the increase in the width of the straight slotted disc. For the simulated fractured loss zones of different widths (2, 4 and 6 mm), the final cumulative loss volume of the MOS plug under 8.0 MPa reached 12.6, 16.2 and 21.8 mL, respectively. Thus, MOS plugging slurry significantly plugged fracture loss zones. Fig. 15a and c presents the blocked straight slotted disc of 2 mm and MOS plug. For the test of 3 mm straight slotted disc, when the experiment was performed out for 35 min, all drilling fluid was suddenly lost. It is speculated that no sufficient strong and tough plug was formed in such wide fracture (Fig. 15b), causing the final destruction of the MOS plug (Fig. 15d) and complete loss of drilling fluid. For this reason, during the use of MOS plugging slurry, the weak bonding strength between the plug and the metal surface should be stressed, in case of failure of cement.

3.5. Permeability recovery

In the presence of severe loss in reservoir, it is most appropriate to directly prepare the MOS plugs by employing water to prevent the insoluble solid particles (e.g., barites) in the drilling fluids from sealing the pores. For losses presenting in cavernous or fractured carbonates with low matrix permeability, the caverns or fractures, i.e., the main oil and gas contribution channels, are capable of completely restoring the flow ability when the MOS cement is dissolved. However, for high permeability rocks (e.g., sandstone), cement particles will also penetrate deep into the pores reducing the permeability. Fig. 16 illustrates the permeability recovery test results. The original permeability of the corundum disc to 2% HEC reached 6522.87 mD. After being damaged by MOS cement, the corundum disc exhibited a reduction of permeability by over 99% (0.25 mD). Fig. 17a and b presents the plugged corundum disc. Subsequently, the corundum disc was soaked in a 15% HCl solution for 2 h at 70 °C, so the MOS cement in the surface could be dissolved (Fig. 17b and c). The permeability regained reached 5412.56 mD, taking up 82.98% of the original permeability. When 15% HCl soak period was extended to 2.5 h to remove the MOS particles in the deep pores, the permeability regained rose to 6135.76 mD, taking up 94.06% of original permeability. As revealed from the result, the solid plug formed by MOS cement could be effectively removed by the acid treatment to regain the permeability of producing zone. The cost of acid treatment could be estimated by complying with the acid concentration and volume used and time consumed for acidizing. In this test, 200 mL of 15% HCl was required to completely dissolve 12 mL of MOS cement in 2 h. The preparation of 1 m^3 15%

Table 5
Density and flow properties of the drilling fluid before and after the addition of solidification additives.

Slurry	Density ρ, g/cm^3	Apparent viscosity, mPa·s	Plastic viscosity, mPa·s	Yield point, Pa	10″/10′ gel strength, Pa
The drilling fluid	1.40	34.5	32	2.40	1/3
MOS plugging slurry	1.43	46	40	5.76	1/3

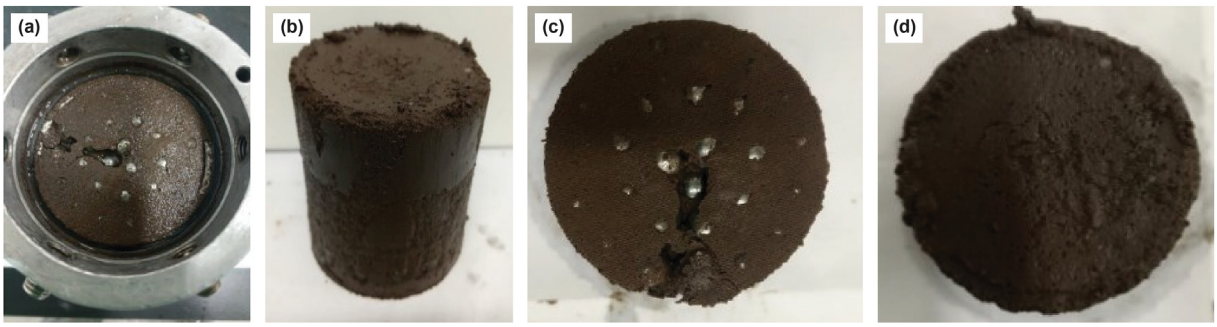

Fig. 13. The state of MOS plug on 10 mm steel ball bed observed from different views: **(a)** bottom view; **(b)** front view; **(c)** bottom view; **(d)** top view.

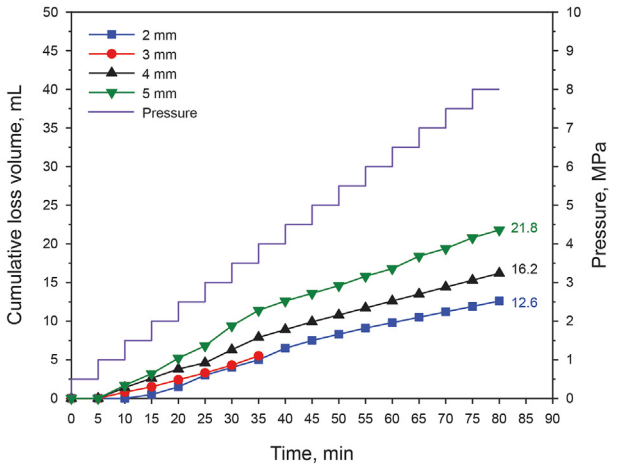

Fig. 14. Cumulative loss volume and plugging pressure versus time for the straight slotted disc with the width of 2, 3, 4 and 5 mm.

HCl solution required 0.449 m^3 31% HCl. Assuming that the cost of 31% HCl is \$53.70/m^3, and the cost of 15% HCl solution is \$21.11. If the dissolution time is within 2 h, the cost of acid treatment for MOS cement is nearly \$351.90/m^3.

3.6. Field application

MOS cement has not been extensively employed as LCM to solve severe loss problems in China. The field case in Well A introduced refers to a successful application of MOS cement in China. Well A located in the Junggar Basin, Xinjiang, is a directional oil well with a designed vertical depth (TV) of 2835 m. The specific parameters are listed in Table 6. Well A suffered multiple losses during the drilling process. The loss history of Well A is presented in Table 7. The two total losses occurred in the Baijiantan Formation at 2177 m and 2192 m and the Kexia Formation at 2555 m. The drilling contractor used high concentration (6%–10%) conventional inert LCMs as the plugging slurry to temporarily reduce the loss rate, and the drilling barely continued. The third total loss occurred in the Carboniferous formation at 2705 m. The drilling contractor employed conventional Class G cement to seal the loss zone of 2129–2705 m. However, when the drilling pipes were tripped again, loss occurred at 1833 m in the Badaowan Formation as impacted by the high density of the drilling fluid. During the redrilling through the cement to 2138 m, total loss occurred again and even up to 15% of inert LCMs could no longer prevent the loss. In the mentioned period, a total volume of over 200 m^3 of drilling fluid was lost.

To plug the well section of 1700–2000 m to resume drilling, MOS cement was used to cure the losses. The following MOS plugging formula was adopted: drilling fluid +3% nut shell (1–3 mm) + 3% nut shell (3–5 mm) + 2% vermiculite (2–5 mm) + 2% comprehensive LCMs + 3% polyacrylamide emulsion + 30% MOS cement, with a density of 1.37 g/cm^3. The plugging operation was elucidated below. First, the drill bit was tripped at 2018 m, and 25.5 m^3 MOS plugging slurry was pumped to the wellbore, and 19 m^3 drilling fluid was displaced at a pump rate of 1.5 m^3/min in 40 min, the MOS plugging slurry was expected to return to the depth of 1700 m. Second, the drill bit was lifted to 1600 m and the cement was waited for curing by 7 h. Third, the shutting process was conducted in the well, and the drilling fluid was pumped with a small rate into the well to determine the pressure bearing capacity of the wellbore, and the downhole pressure difference was 2.2 MPa, and the stable pressure difference

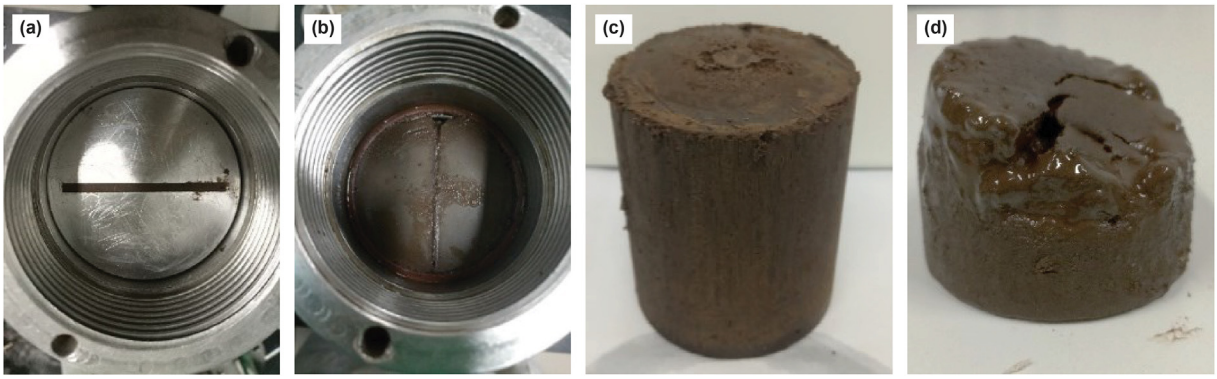

Fig. 15. **(a)** Blocked straight slotted disc of 2 mm from bottom view of the drilling cup; **(b)** MOS plug after removing the straight slotted disc of 3 mm from the bottom view of the drilling cup; **(c)** MOS plug after plugging the straight slotted disc of 2 mm (front view); **(d)** destroyed MOS plug after plugging the straight slotted disc of 3 mm (front view).

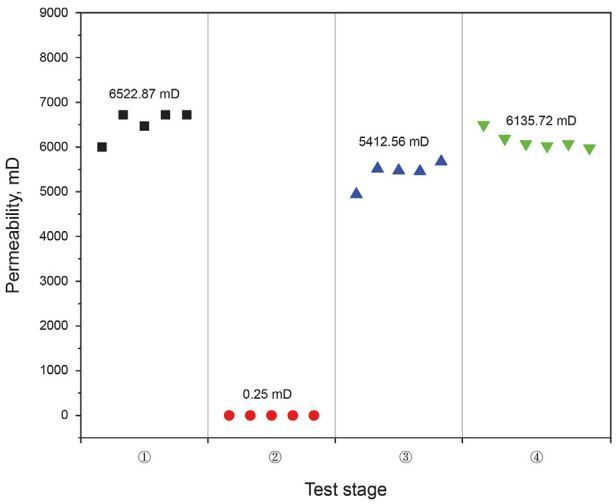

Fig. 16. Permeability recovery test of the corundum disc: ① initial flow of 2% HEC; ② 2% HEC injection after damaged by MOS cement; ③ 2% HEC injection after 2 h soaked in 15% HCl solution ④ 2% HEC injection after 2.5 h soaked in 15% HCl solution.

was 1.5 MPa. In the subsequent drilling, the density of the drilling fluid increased to 1.37 g/cm^3, and no loss occurred again.

Given the drilling process, the loss interval of this well was from 1734 m to 2705 m. As impacted by the high permeability of the sandstone formation and the existence of natural fractures, the conventional LCMs cannot effectively stay under the condition of wellbore fluid washout and formation fluid erosion, as shown in Fig. 18. So the blocking layer is easy to dilute and wash away, thereby causing repeated losses. The loss treatment with Class G cement requires specific devices (e.g., cement tanker and pump truck). Besides, the time of waiting on cement is as long as 24–48 h (Lavrov, 2016). When using MOS cement as LCM, it was directly mixed in the drilling fluid tank and the plugging slurry was pumped by the drilling fluid pump. After solidification in the loss zones, the MOS plug can resist the pressure disturbance, thus effectively reducing the repeated losses and improving the pressure bearing capacity of the loss zones. In addition, the total plugging operation time was only 10 h, so the cost was down-regulated. The successful application in well A in the Junggar Basin, Xinjiang shows that MOS cement is characterized by operability, short waiting on cement time and good effect of plugging and a good application prospect.

4. Conclusions

In the present study, MOS cement was developed as a lost circulation material to solve losses that occur in porous or fractured loss zones. The compressive strength development mechanism of MOS cement at 70 °C for 24 h was revealed by phase composition and microstructure analysis. The retarding effects of citric acid, boric acid and borax for MOS cement were compared and then optimized. In addition, the plugging performance of MOS plugging slurry for simulated large porous zone and fractured zone was evaluated. Moreover, a core permeability recovery test was performed to evaluate the degree of formation damage. The successful field application of MOS cement was introduced. Given the results, the following conclusions are drawn:

(1) The main crystal-phases formed in MOS cement at 70 °C for 24 h are $Mg(OH)_2$ and $5Mg(OH)_2 \cdot MgSO_4 \cdot 2H_2O$ (5-1-2 phase). Higher molar ratio of $MgO/MgSO_4 \cdot 7H_2O$ and lower molar ratio of $H_2O/MgSO_4 \cdot 7H_2O$ are conducive to high

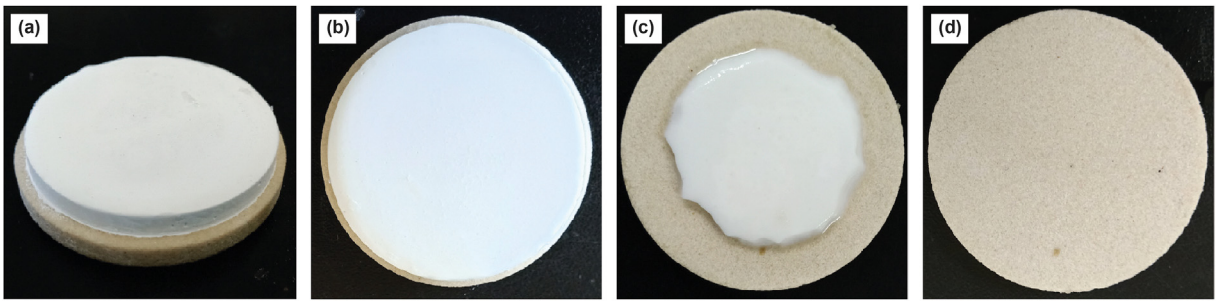

Fig. 17. Corundum disc after being damaged by MOS cement: **(a)** front view; **(b)** top view; **(c)** soaked in 15% HCl after 1 h; **(d)** soaked in 15% HCl after 2 h.

Table 6
Casing program of Well A.

Drilling order	Bit size, mm	Well Section, m	Casing size, mm	Casing depth, m	Altitude of cement loop, m
First section	381.00	0–381.00	273.10	300.00	0–300.00
Second section	243.30	381.00–2140.00	193.70	0–3078.49	1840–3078.49
	215.90	2140.00–3078.49			

Note: the depth of kickoff point is 1243.00 m and the deviation is 35.54° at the well depth of 2705.00 m.

Table 7
Loss history of Well A.

Number	Loss depth, m	Loss zones	Drilling fluid density, g/cm^3	Loss degree	Loss treatments
1	2177, 2192	Baijiantan	1.28	Total loss	Conventional lost circulation materials (concentration: 6%–8%)
2	2555	Kexia	1.27	Total loss	Conventional lost circulation materials (concentration: 10%)
3	2705	Carboniferous	1.34	Total loss	Class G well cement (cement depth: 2129 m)
4	1740, 1833	Badaowan	1.24	partial loss	Conventional lost circulation materials (concentration: 5%)
5	2138, 2150 (Redrilling)	Baijiantan	1.31	Total loss	Conventional lost circulation materials (concentration: 15%)

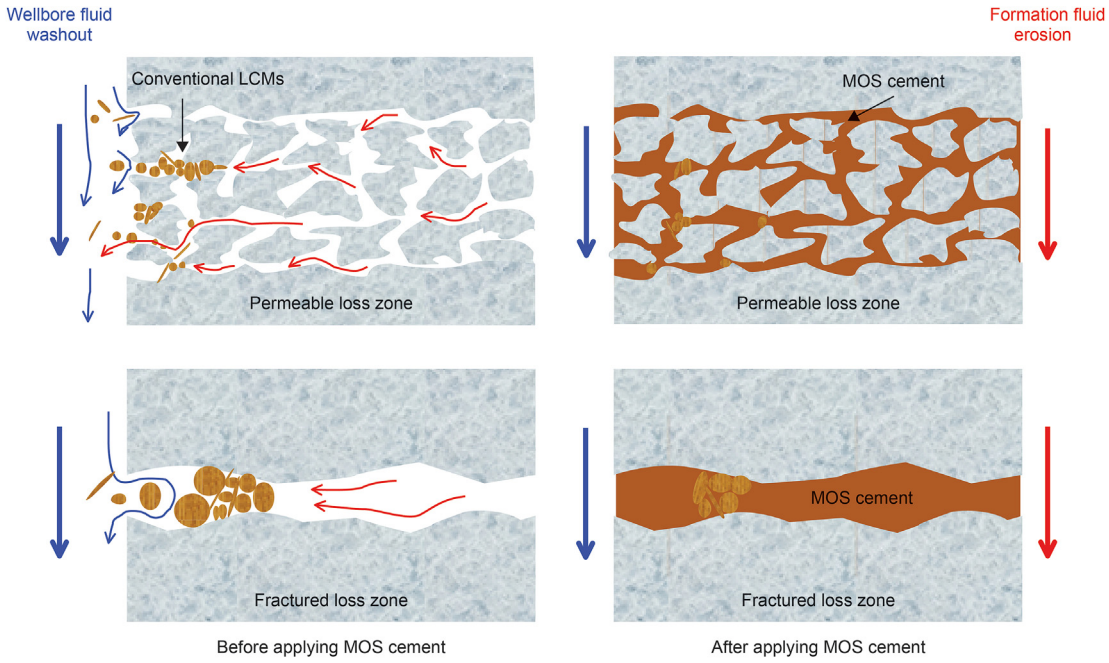

Fig. 18. Plugging effects before and after applying MOS cement in the permeable loss zone and the fractured loss zone.

compressive strength, consistent with that at ambient temperature.

(2) Citric acid, boric acid and borax all exert a retarding effect on MOS cement at 70 °C. Their retarding ability is ranked as: boric acid > borax > citric acid.

(3) The MOS plugging slurry can be prepared from distilled water or in-situ field drilling fluid. For in-situ field drilling fluid, the optimized MOS plugging slurry formula is: the drilling fluid +26% main agent (MgO and $MgSO_4 \cdot 7H_2O$) + 6.5% retarder (borax), with a high plugging ability for large porous loss zone simulated by two layer steel ball beds with diameters from 8 to 10 mm and fractured loss zone simulated by straight slotted discs with widths from 2 to 5 mm.

(4) The MOS cement exhibits an acid solubility of almost 100%. The permeability regained is 94.06% after the MOS cement on the core is removed by 15% HCl solution, which indicates that MOS cement can be removed by acid treatment to effectively regain the permeability of producing zone.

(5) The successful field application of MOS cement in a well in the Junggar Basin, Xinjiang, China verifies the good plugging effect of MOS cement for severe losses.

Acknowledgements

This work was supported by the National Natural Science Foundation (Grant No. 51874329 and Grant No. 52004297 and Grant No. 51991361), the National Natural Science Innovation Population of China (Grant No.51821092), the Strategic Cooperation Technology Projects of CNPC and CUPB (Grant No. ZLZX2020-01) and Cooperation projects of CCDC and CUPB (CQ2021B-33-Z2-3).

Appendix

1. The measured content of oxides and ignition loss contained in the light-burned MgO powder is listed in Table A1, which was provided by Hebei Magnesium Chemical Technology Co. Ltd. (China). The impurities of light-burned MgO includes $MgCO_3$ (PDF card no. 86–2344), SiO_2 (PDF card no. 79–0563) and $Mg_3(OH)_2Si_4O_{10}$ (PDF card no. 13–2558) measured by the X-Ray Diffraction (XRD) (Fig. A1).

Table A1
Main components of light-burned MgO

Component	MgO	Al_2O_3	Fe_2O_3	SiO_2	CaO	Ignition loss	Others
Content, %	87.50	0.16	0.41	2.98	1.06	2.30	5.59

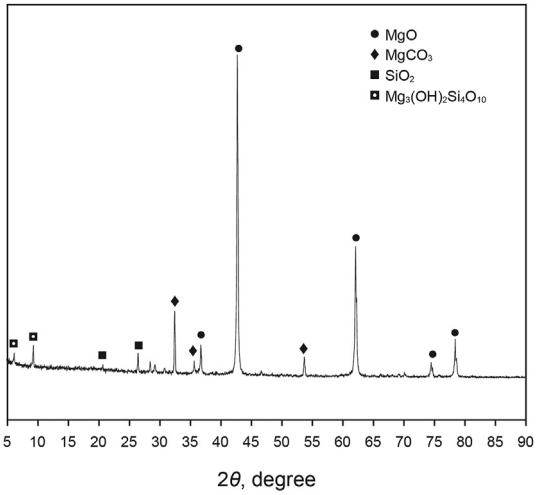

Fig. A1. X-ray diffraction pattern of light-burned MgO.

2. The light-burned MgO has a mean particle size of 12.095 μm measured by the particle size analysis (Fig. A2).

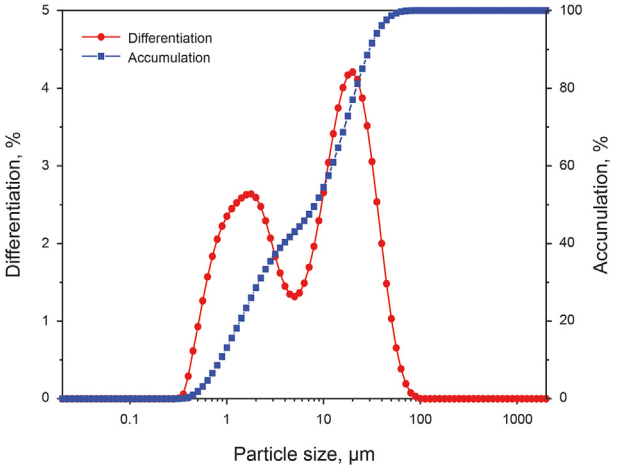

Fig. A2. The PSA of light-burned MgO.

3. The activity of MgO is 53.7% measured by hydration method, the test procedure is as follows:

First, accurately weighed 2.0 g of light-burned MgO was placed in a φ40 mm × 25 mm glass weighing bottle containing 20 mL distilled water, which was covered by the lid for hydration at a temperature of 20 ± 2 °C and a relative humidity of 70 ± 5% for 24 h. Then, the bottle was pre-dried in an oven at 100–110 °C, followed by raising the oven temperature to 150 °C until the sample reached a constant weight. Lastly, it was taken out and cooled to ambient temperature, and the weight after hydration of the sample was weighed. The MgO activity is given by:

$$Activity = \frac{m_2 - m_1}{0.45 m_1} \times 100\% \quad (1)$$

where m_1, m_2 are the initial weight of MgO and that after drying, respectively, g.

So, the actual activity of MgO is:

$$Activity = \frac{2.483 - 2.000}{0.45 \times 2.000} \times 100\% = 53.7\% \quad (2)$$

References

Abrams, A., 1977. Mud design to minimize rock impairment due to particle invasion. J. Petrol. Technol. 29 (5), 586–592. https://doi.org/10.2118/5713-PA.

Ahmed, T., 2010. Reservoir Engineering Handbook, Fourth ed. Gulf Professional Publishing, Burlington https://doi.org/10.1016/C2009-0-30429-8.

Alkinani, H.H., Al-Hameedi, A.T.T., Dunn-Norman, S., Al-Bazzaz, W.H., 2020. State-of-the-art review of lost circulation materials and treatments – Part II: probability and cost analyses. International Petroleum Technology Conference, Dhahran, Kingdom of Saudi Arabia, 13-15 January. Society of Petroleum Engineers. https://doi.org/10.2523/IPTC-19877-MS.

Alsaba, M., Nygaard, R., Hareland, G., Contreras, O., 2014a. Review of lost circulation materials and treatments with an updated classification. AADE National Technical Conference and Exhibition, Texas, Houston, USA.

Alsaba, M., Nygaard, R., Saasen, A., Nes, O.M., 2014b. Laboratory evaluation of sealing wide fractures using conventional lost circulation materials. SPE Annual Technical Conference and Exhibition, Amsterdam, The Netherlands, 27-29 October. Society of Petroleum Engineers. https://doi.org/10.2118/170576-MS.

American Petroleum Institute, 2009. Recommended Practice for Field Testing Water-Based Drilling Fluids, Fourth ed. Washington D.C., USA. API 13B-1.

Arora, A., 2005. Text Book of Inorganic Chemistry. Discovery Publishing House, India.

Barralet, J., Grover, L., Gbureck, U., 2004. Ionic modification of calcium phosphate cement viscosity. Part II: hypodermic injection and strength improvement of brushite cement. Biomaterials 25 (11), 2197–2203. https://doi.org/10.1016/j.biomaterials.2003.09.085.

Beaudoin, J.J., Ramachandran, V.S., 1978. Strength development in magnesium oxysulfate cement. Cement Concr. Res. 8 (1), 103–112. https://doi.org/10.1016/0008-8846(78)90063-7.

Bour, D., Vinson, E., Totten, P., Waheed, A., 1993. Low-density acid-removable cement as a solution for lost circulation across producing formations. Middle East Oil Show, Bahrain, 3-6 April. Society of Petroleum Engineers. https://doi.org/10.2118/25543-MS.

Caenn, R., Darley, H.C., Gray, G.R., 2017. Composition and Properties of Drilling and Completion Fluids, Seventh ed. Gulf professional Publishing, MA https://doi.org/10.1016/C2015-0-04159-4.

Chellappah, K., Aston, M., Maltby, T., Savari, S., Whitfill, D.L., 2018. Engineered nutshell particles for wellbore strengthening. IADC/SPE Drilling Conference and Exhibition, Fort Worth, Texas, USA, 6-8 March. Society of Petroleum Engineers. https://doi.org/10.2118/189574-MS.

Ciriminna, R., Meneguzzo, F., Delisi, R., Pagliaro, M., 2017. Citric acid: emerging applications of key biotechnology industrial product. Chem. Cent. J. 11 (1), 22. https://doi.org/10.1186/s13065-017-0251-y.

Cole-Hamilton, W.M., Curtis, J.A., 2008. Chemical intervention technology for low-risk annular isolation in existing gravel packed wells and uncemented annuli. In: SPE Annual Technical Conference and Exhibition, Denver, Colorado, USA, 21-24 September. Society of Petroleum Engineers. https://doi.org/10.2118/115254-MS.

Cui, K., Jiang, G., Quan, X., Wang, Z., Hua, Z., August 2020. Study of effects of downhole conditions on the setting time and compressive strength of MOS settable system by orthogonal experimental design. The 6th International Conference on Water Resource and Environment. IOP Publishing, Toyko, Japan, pp. 23–26. https://doi.org/10.1088/1755-1315/612/1/012011.

David, M.G., Charles, D.W., 1986. Terpolymer Composition for Aqueous Drilling Fluids. US Patent No, p. 4678591.

Demediuk, T., Cole, W., 1957. A study of mangesium oxysulphates. Aust. J. Chem. 10 (3), 287–294. https://doi.org/10.1071/CH9570287.

Dick, M.A., Heinz, T.J., Svoboda, C.F., Aston, M., 2000. Optimizing the selection of bridging particles for reservoir drilling fluids. SPE International Symposium on Formation Damage Control, Lafayette, Louisiana, USA, 23-24 February. Society of Petroleum Engineers. https://doi.org/10.2118/58793-MS.

Ekholm, P., Virkki, L., Ylinen, M., Johansson, L., 2003. The effect of phytic acid and some natural chelating agents on the solubility of mineral elements in oat bran. Food Chem. 80 (2), 165–170. https://doi.org/10.1016/S0308-8146(02)00249-2.

Elkatatny, S., Ahmed, A., Abughaban, M., Patil, S., 2020. Deep illustration for loss of circulation while drilling. Arabian J. Sci. Eng. 45, 483–499. https://doi.org/10.1007/s13369-019-04315-6.

Fu, J., Liang, W., Wang, H., He, Z., 2011. Synthesis and characterization of $MgSO_4 \cdot 5Mg(OH)_2 \cdot 2H_2O$ flake powders. J Cent South Univ Technol 18 (6), 1871–1876. https://doi.org/10.1007/s11771-011-0916-y.

Gates-Rector, S., Blanton, T., 2019. The Powder Diffraction File: a quality materials characterization database. Powder Diffr. 34 (4), 352–360. https://doi.org/10.1017/S0885715619000812.

Gbureck, U., Barralet, J.E., Spatz, K., Grover, L.M., Thull, R., 2004. Ionic modification of calcium phosphate cement viscosity. Part I: hypodermic injection and strength improvement of apatite cement. Biomaterials 25 (11), 2187–2195. https://doi.org/10.1016/j.biomaterials.2003.08.066.

Hall, D.A., Stevens, R., El-Jazairi, B., 2001. The effect of retarders on the microstructure and mechanical properties of magnesia–phosphate cement mortar. Cement Concr. Res. 31 (3), 455–465. https://doi.org/10.1016/S0008-8846(00)00501-9.

Howard, G.C., Scott Jr., P.P., 1951. An analysis and the control of lost circulation. J. Petrol. Technol. 3 (6), 171–182. https://doi.org/10.2118/951171-G.

Jadhav, R., Patil, S., 2018. Acid-soluble thixotropic cement system for lost circulation challenges. In: Abu Dhabi International Petroleum Exhibition & Conference, Abu Dhabi, UAE, 12-15 November. Society of Petroleum Engineers. https://doi.org/10.2118/193168-MS.

Jeroch, W., 1906. Magnesium Cement and Process of Manufacturing Same. US Patent No, p. 833930A.

Johannes, K.F., 2012. Petroleum Engineer's Guide to Oil Field Chemicals and Fluids. Gulf Professional Publishing, Waltham.

Kumar, A., Savari, S., Whitfill, D., Jamison, D.E., 2010. Wellbore strengthening: the less-studied properties of lost-circulation materials. SPE Annual Technical Conference and Exhibition, Florence, Italy, 19-22 September. Society of Petroleum Engineers. https://doi.org/10.2118/133484-MS.

Lavrov, A., 2016. Lost Circulation Mechanisms and Solutions. Gulf Professional Publishing, Amsterdam.

Li, W., Liu, J., Zhao, X., Yang, C., Zhang, J., Li, Y., Peng, H., Lv, D., 2018. Effect of flushing fluid composition on rate of penetration in limestone: surface and interface aspects. The 1st International Conference on Advances in Rock Mechanics - TuniRock 2018, Hammamet, Tunisia Hammamet, Tunisia, 29-31 March. Society for Rock Mechanics, ISRM-TUNIROCK-2018-18.

Li, W., Zhao, X., Li, Y., Ji, Y., Peng, H., Liu, L., Yang, Q., 2015. Laboratory investigations on the effects of surfactants on rate of penetration in rotary diamond drilling. J. Petrol. Sci. Eng. 134, 114–122. https://doi.org/10.1016/j.petrol.2015.07.027.

Li, Z., Ji, Z., 2015. Effect of molar ratios on compressive strength of modified magnesium oxysulfate cement. Int J Hybrid Inf Technol 8 (6), 87–94. https://doi.org/10.14257/ijhit.2015.8.6.09.

Li, Z., Ji, Z., Jiang, L., Yu, S., 2017. Effect of additives on the properties of magnesium oxysulfate cement. J. Intell. Fuzzy Syst. 33 (5), 3021–3025. https://doi.org/10.3233/JIFS-169353.

Luke, K., Soucy, K.S., 2008. Test method to optimize acid-soluble cement for

unconventional gas completions. In: CIPC/SPE Gas Technology Symposium 2008 Joint Conference, Calgary, Alberta, Canada, 16-19 June. Society of Petroleum Engineers. https://doi.org/10.2118/114759-MS.
Mata, F., Veiga, M., 2004. Crosslinked cements solve lost circulation problems. SPE Annual Technical Conference and Exhibition, Texas, Houston, USA, 26-29 September. Society of Petroleum Engineers. https://doi.org/10.2118/90496-MS.
Müller, U.F., Tor, Y., 2014. Citric acid and the RNA world. Angew. Chem. Int. Ed. 53 (21), 5245–5247. https://doi.org/10.1002/anie.201400847.
Nasiri, A., Ghaffarkhah, A., Dijvejin, Z.A., Mostofi, M., Moraveji, M.K., 2018. Bridging performance of new eco-friendly lost circulation materials. Petrol. Explor. Dev. 45 (6), 1154–1165. https://doi.org/10.1016/S1876-3804(18)30119-8.
Nayberg, T., 1987. Laboratory study of lost circulation materials for use in both oil-based and water-based drilling muds. SPE Drill. Eng. 2 (3), 229–236. https://doi.org/10.2118/14723-PA.
Newman, E., 1964. Preparation and heat of formation of a magnesium oxysulfate. J Res Natl Bur Stand A Phys Chem 68A (6), 645–650. https://doi.org/10.6028/jres.068A.064.
Onyia, E.C., 1994. Experimental data analysis of lost-circulation problems during drilling with oil-based mud. SPE Drill. Complet. 9 (1), 25–31. https://doi.org/10.2118/22581-PA.
Qin, L., Gao, X., Li, W., Ye, H., 2018. Modification of magnesium oxysulfate cement by incorporating weak acids. J. Mater. Civ. Eng. 30 (9), 04018209. https://doi.org/10.1061/(ASCE)MT.1943-5533.0002418.
Ravi, K., 2010. Successful Application of acid soluble plugs in open hole slotted liner completion. SPE Oil and Gas India Conference and Exhibition, Mumbai, India, 20-22 January. Society of Petroleum Engineers. January. https://doi.org/10.2118/129159-MS.
Rueff, E., 1907. Magnesium Cement and Process of Making the Same. US Patent No, p. 872375.
Savari, S., Kulkarni, S.D., Whitfill, D.L., Jamison, D.E., 2015. Engineering' design of lost circulation materials (LCMs) is more than adding a word. SPE/IADC Drilling Conference and Exhibition, London, England, UK, 17-19 March. Society of Petroleum Engineers. https://doi.org/10.2118/173018-MS.
Seymour, B., Santra, A., 2013. Detailed laboratory investigation of acid soluble cements as solution for lost circulation across the producing zones. In: SPE/IADC Middle East Drilling Technology Conference & Exhibition, Dubai, UAE, 7-9 October. Society of Petroleum Engineers. https://doi.org/10.2118/166804-MS.
Stewart, L., 1932. Magnesia Cement Composition. US Patent No, p. 1853522.
Sugama, T., Kukacka, L., 1983. Characteristics of magnesium polyphosphate cements derived from ammonium polyphosphate solutions. Cement Concr. Res. 13 (4), 499–506. https://doi.org/10.1016/0008-8846(83)90008-x.
Sugama, T., Kukacka, L., Warren, J., Galen, B., 1986. Bentonite-based ammonium polyphosphate cementitious lost-circulation control materials. J. Mater. Sci. 21 (6), 2159–2168. https://doi.org/10.1007/bf00547964.
Sweatman, R.E., Scoggins, W.C., 1990. Acid-soluble magnesia cement: new applications in completion and workover operations. SPE Prod. Eng. 5 (4), 441–447. https://doi.org/10.2118/18031-PA.
Urwongse, L., Sorrell, C.A., 1980. Phase relations in magnesium oxysulfate cements. J. Am. Ceram. Soc. 63 (9–10), 523–526. https://doi.org/10.1111/j.1151-2916.1980.tb10757.x.
Vickers, S., Cowie, M., Jones, T., Twynam, A.J., 2006. A new methodology that surpasses current bridging theories to efficiently seal a varied pore throat distribution as found in natural reservoir formations. Wierntnictwo, Nafta, Gaz. 23 (1), 501–515.
Vinson, E., Totten, P., Middaugh, R., 1992. Acid removable cement system helps lost circulation in productive zones. In: SPE/IADC drilling conference, New Orleans, Louisiana, USA, 18-21 February. Society of Petroleum Engineers. https://doi.org/10.2118/23929-MS.
Walling, S.A., Provis, J.L., 2016. Magnesia-based cements: a journey of 150 years, and cements for the future? Chem. Rev. 116 (7), 4170–4204. https://doi.org/10.1021/acs.chemrev.5b00463.
Wang, H., Sweatman, R.E., Engelman, R.E., Deeg, W.F., Whitfill, D.L., 2005. The key to successfully applying today's lost circulation solutions. SPE Annual Technical Conference and Exhibition, Dallas, Texas, USA, 9-12 October. Society of Petroleum Engineers. https://doi.org/10.2118/95895-MS.
Wang, J., 2007. Research on Automatic Lost Circulation Prevention Technology of the Functional Compound Gel. Sichuan University, Chengdu.
Wang, N., Yu, H., Bi, W., Tan, Y., Zhang, N., Wu, C., Ma, H., Hua, S., 2018. Effects of sodium citrate and citric acid on the properties of magnesium oxysulfate cement. Construct. Build. Mater. 169, 697–704. https://doi.org/10.1016/j.conbuildmat.2018.02.208.
Wang, S., Xu, C., Yu, S., Wu, X., Jie, Z., Dai, H., 2019. Citric acid enhances the physical properties, cytocompatibility and osteogenesis of magnesium calcium phosphate cement. J Mech Behav Biomed Mater 94, 42–50. https://doi.org/10.1016/j.jmbbm.2019.02.0.
Werner, B., Myrseth, V., Saasen, A., 2017. Viscoelastic properties of drilling fluids and their influence on cuttings transport. J. Petrol. Sci. Eng. 156, 845–851. https://doi.org/10.1016/j.petrol.2017.06.063.
Whitfill, D.L., Hemphill, T., 2003. All lost-circulation materials and systems are not created equal. SPE Annual Technical Conference and Exhibition, Denver, Colorado, USA, 5-8 October. Society of Petroleum Engineers. https://doi.org/10.2118/84319-MS.
Wu, C., Yu, H., Dong, J., Zheng, L., 2014. Effects of material ration, fly Ash, and citric acid on magnesium oxysulfate cement. ACI Mater. J. 111 (3), 291–297. https://doi.org/10.14359/51686723.
Xu, C., Yan, X., Kang, Y., You, L., Zhang, J., 2020. Structural failure mechanism and strengthening method of fracture plugging zone for lost circulation control in deep naturally fractured reservoirs. Petrol. Explor. Dev. 47 (2), 430–440. https://doi.org/10.1016/S1876-3804(20)60060-X.
Zeng, X., Yu, H., Wu, C., 2019. An overview of study on basic magnesium sulfate cement and concrete in China (2012–2019). KSCE J Civ Eng 23 (10), 4445–4453. https://doi.org/10.1007/s12205-019-0199-7.